

Suppression of superconductivity in layered $\text{Bi}_4\text{O}_4\text{S}_3$ by Ag doping

S.G. Tan¹, P. Tong¹, Y. Liu¹, W.J. Lu¹, L.J. Li¹, B.C. Zhao¹, and Y.P. Sun^{1,2,a}

¹ Key Laboratory of Materials Physics, Institute of Solid State Physics, Chinese Academy of Sciences, Hefei 230031, P.R. China

² High Magnetic Field Laboratory, Chinese Academy of Sciences, Hefei 230031, P.R. China

Received 3 September 2012

Published online (Inserted Later) – © EDP Sciences, Società Italiana di Fisica, Springer-Verlag 2012

Abstract. We report X-ray diffraction, magnetization and transport measurements for polycrystalline samples of the new layered superconductor $\text{Bi}_{4-x}\text{Ag}_x\text{O}_4\text{S}_3$ ($0 \leq x \leq 0.2$). The superconducting transition temperature (T_C) decreases gradually and finally suppressed when $x < 0.10$. Accordingly, the resistivity changes from a metallic behavior for $x < 0.1$ to a semiconductor-like behavior for $x > 0.1$. The analysis of Seebeck coefficient shows there are two types of electron-like carriers dominate at different temperature regions, indicative of a multiband effect responsible for the transport properties. The suppression of superconductivity and the increased resistivity can be attributed to a shift of the Fermi level to the lower-energy side upon doping, which reduces the density of states at E_F . Further, our result indicates the superconductivity in $\text{Bi}_4\text{O}_4\text{S}_3$ is intrinsic and the dopant Ag prefers to enter the BiS_2 layers, which may essentially modify the electronic structure.

1 Introduction

To study the layered materials is one of the strategies for exploring new superconductors. The discoveries of superconductivity with high superconducting transition temperature (T_C) in cuprates and oxypnictides have given us good examples [1–6]. In those compounds, the CuO_2 layer or the Fe_2An_2 ($\text{An} = \text{P}, \text{As}, \text{Se}, \text{Te}$) layer plays a central role in determining the superconductivity. Very recently, Mizuguchi et al., reported the superconductivity in layered Bismuth oxy-sulfide $\text{Bi}_4\text{O}_4\text{S}_3$ with $T_C \sim 4.5$ K [7]. Structurally, $\text{Bi}_4\text{O}_4\text{S}_3$ is composed of a stacking of $\text{Bi}_4\text{O}_4(\text{SO}_4)_{0.5}$ spacer layers and two BiS_2 layers [7]. There are 50% defects on SO_4 sites in $\text{Bi}_4\text{O}_4\text{S}_3$, while the parent compound $\text{Bi}_6\text{O}_8\text{S}_5$ free of SO_4 defects is an insulator [7]. Band structure calculation indicates the Fermi level lies within the bands mainly originating from the Bi $6p$ orbitals within the BiS_2 layer in $\text{Bi}_4\text{O}_4\text{S}_3$. So the BiS_2 layer was believed to be a basic unit as the CuO_2 layer in cuprates or the Fe_2An_2 layer in oxypnictides [7]. Since the discovery of superconductivity, $\text{Bi}_4\text{O}_4\text{S}_3$ has attracted increasing attention because it could stimulate extensive investigations on the BiS_2 based layered compounds for exploring new high- T_C superconductors [8–13]. The Hall coefficient measurements indicate an exotic multi-band behavior and the charge carriers are mainly electron-type [8], which is consistent with our

Seebeck coefficient measurement [9]. Our magnetization measurement implies that $\text{Bi}_4\text{O}_4\text{S}_3$ is a typical type-II superconductor [9]. The characterizations based on the polycrystalline samples with impurities, such as Bi and Bi_2O_3 , indicated a bulk superconducting behavior [10,11]. However, the almost pure sample synthesized by high pressure does not exhibit superconductivity down to 2 K [12], which may be attributable to the local structure distortion formed in the high-pressure synthesized sample. It is therefore questionable whether the observed superconductivity in $\text{Bi}_4\text{O}_4\text{S}_3$ is intrinsic. Chemical doping that usually serves as a powerful way to study the underlying physics of superconductivity, however, has not been reported up to date. Here we report our systematical structural, magnetic, electrical and thermal transport measurements for Ag doped $\text{Bi}_{4-x}\text{Ag}_x\text{O}_4\text{S}_3$ ($0 \leq x \leq 0.2$). The lattice shrinks gradually with Ag doping. The T_C is reduced and finally suppressed for $x > 0.1$. Accompanying the suppression of superconductivity, the resistivity is increased remarkably and behaves as a semiconductor for $x > 0.1$, attributable to a shift of the Fermi energy (E_F) demonstrated by the analysis of Seebeck coefficient. For all samples, the Seebeck coefficient is linearly temperature dependent at both low- and high-temperature regions with different slopes, indicating a multiband behavior. Moreover, our results demonstrate that the superconductivity in $\text{Bi}_4\text{O}_4\text{S}_3$ is intrinsic and the dopant Ag enters the BiS_2 layer rather than the impurity Bi phase.

^a e-mail: ypsun@issp.ac.cn

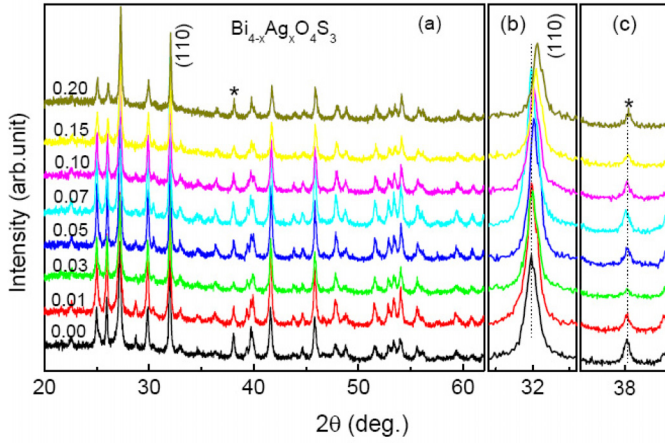


Fig. 1. (Color online) (a) The X-ray diffractions for $\text{Bi}_{4-x}\text{Ag}_x\text{O}_4\text{S}_3$ ($0 \leq x \leq 0.2$). One diffraction peak from impurity Bi was marked by the asterisk. The area of the (110) peak for $\text{Bi}_{4-x}\text{Ag}_x\text{O}_4\text{S}_3$ is enlarged in (b), and that of the Bi diffraction peak in (c).

2 Experimental details

The Ag (4N), Bi (3N), S (3N) and Bi_2O_3 (>3N) powders in stoichiometric ratio were fully mixed and ground, and then pressed into pellets [9]. The pellets were sealed in an evacuated silica tube. The tube was heated at 450 °C for 10 h, and then at 510 °C for another 10 h. The obtained pellets were ground again and the above treatment was repeated. The room-temperature crystal structure and lattice constants were determined by powder X-ray diffraction (XRD) (Philips X'pert PRO) with Cu K_α radiation. The electronic and thermal transport measurements were performed in a Quantum Design physical property measurement system (PPMS), and the magnetization measurement was performed on a superconducting quantum interference device (SQUID) system.

3 Experimental results and discussion

In Figure 1a, the XRD patterns are shown for the polycrystalline $\text{Bi}_{4-x}\text{Ag}_x\text{O}_4\text{S}_3$ ($0 \leq x \leq 0.2$) samples. The Bragg diffractions can be indexed using the tetragonal structure with the space group of $I4/mmm$ [7]. The diffractions from the impurity Bi were also observed and one of them was marked by the asterisk. The diffractions from the $\text{Bi}_{4-x}\text{Ag}_x\text{O}_4\text{S}_3$ show a dependence on the Ag concentration x , while those from Bi do not. For instance, the (110) peak of $\text{Bi}_{4-x}\text{Ag}_x\text{O}_4\text{S}_3$ shifts clearly towards the higher angles as x increases, as seen in Figure 1b. As shown in Figure 1c, however, the position and intensity of the Bi peak are unchangeable with x . This indicates that the dopant Ag indeed enters the $\text{Bi}_4\text{O}_4\text{S}_3$ lattice. The lattice parameters for $\text{Bi}_{4-x}\text{Ag}_x\text{O}_4\text{S}_3$ are obtained by a standard Rietveld refinement for the powder XRD patterns using the Rietica software [14]. As a result, both the lattice constant a ($=b$) and c decrease with increasing Ag content, as plotted in Figure 2.

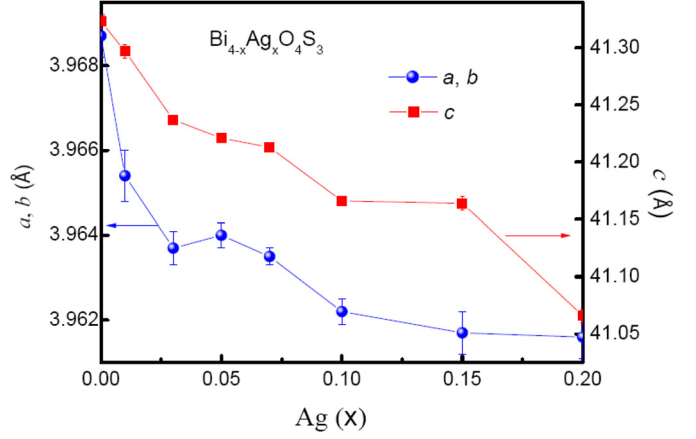


Fig. 2. (Color online) The refined lattice constants for $\text{Bi}_{4-x}\text{Ag}_x\text{O}_4\text{S}_3$ ($0 \leq x \leq 0.2$). The error bars were generated by the Rietveld refinement.

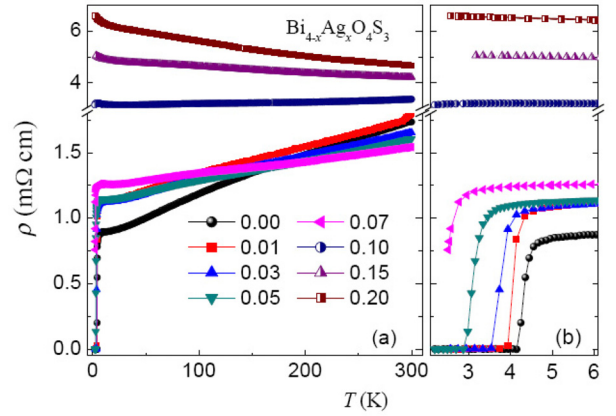


Fig. 3. (Color online) (a) The resistivity for $\text{Bi}_{4-x}\text{Ag}_x\text{O}_4\text{S}_3$ ($0 \leq x \leq 0.2$) as a function of temperature. (b) An enlarged view for the low-temperature resistivity curves.

The temperature dependence of the resistivity $\rho(T)$ for $\text{Bi}_{4-x}\text{Ag}_x\text{O}_4\text{S}_3$ was measured by a standard four-probe method under a zero magnetic field. As displayed in Figure 3a, the metallic $\rho(T)$ shape at $x = 0$ changes gradually to a semiconducting one when $x > 0.10$, accompanying an increase of the entire resistivity. Meanwhile, the superconducting transition temperature is reduced with increasing x and non superconductivity can be found down to 2 K for $x > 0.1$ (Fig. 3b). The magnetic susceptibility $4\pi\chi(T)$ is displayed in Figure 4. In good agreement with the resistivity result, the superconducting transition temperature decreases as x increases. Simultaneously, the shielding volume fraction, determined as the value of $-4\pi\chi$ at 2 K, reduces from $-0.45 \text{ emu}/(\text{cm}^3 \text{ Oe})$ for $x = 0$ to $-3 \times 10^{-4} \text{ emu}/(\text{cm}^3 \text{ Oe})$ for $x = 0.07$, above which the superconductivity, even if exists, lost its bulk characteristics. The superconducting transition temperatures defined by different ways will be discussed in the following text.

The Seebeck coefficient $S(T)$ is plotted in Figure 5a for selected samples. The $S(T)$ is negative in the entire temperature range up to 320 K, indicating the major carriers are electron-like for all samples. As shown in the inset

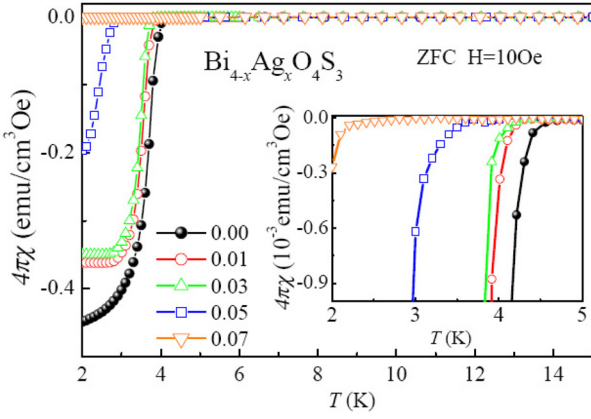


Fig. 4. (Color online) Temperature dependence of the magnetic susceptibility $4\pi\chi(T)$ for $\text{Bi}_{4-x}\text{Ag}_x\text{O}_4\text{S}_3$ ($0 \leq x \leq 0.07$) at $H = 10$ Oe. Inset shows the details of the $4\pi\chi(T)$ curves around the T_C .

of Figure 5a, the Seebeck coefficient at 320 K, $S_{320\text{K}}$, increases as x increases and a sharp enhancement happens at $\sim x = 0.10$, consistent with the increasing resistivity and the appearance of the semiconductor-like behavior for $x > 0.1$ (Fig. 3). Generally, the $S(T)$ consists of three different parts: the diffusion term, the spin-dependent scattering term and the phonon-drag term due to electron-phonon interaction [15]. The spin-dependent contribution is probably very weak since there are no magnetic elements in $\text{Bi}_{4-x}\text{Ag}_x\text{O}_4\text{S}_3$. The phonon-drag effect gives $\sim T^3$ dependence for $T \ll \Theta_D$, and $\sim 1/T$ for $T \geq \Theta_D$ (where Θ_D is the Debye temperature), and thus a phonon-drag peak in $S(T)$ at $\sim \Theta_D/5$ [15]. The Θ_D is 192 K for the undoped sample derived from heat capacity measurement [10]. However, the expected peak structure at $\sim \Theta_D/5 = 38$ K is absent and the high-temperature $S(T)$ does not obey the $\sim 1/T$ expression, indicating the phonon contribution is considerably weak in the current samples. Usually, the diffusion term gives rise to a linearly temperature dependent $S(T)$ at low temperatures [15], which is actually observed and shown in Figure 5b (for clarity, only the data for $x = 0$ and 0.2 are shown). Interestingly, at higher temperatures the $S(T)$ for all samples exhibit another linear temperature dependence with a different slope. For instance, the cases of $x = 0$ and $x = 0.2$ were shown in the same figure. The high-temperature linear behavior of $S(T)$ may indicate a different type of dominant charge diffusion contributing to the high-temperature $S(T)$. The extrapolations of the linear $S(T)$ portions at both low and high temperatures cross at some temperatures, marked as T^* . The T^* is found to be almost constant for $x < 0.10$ within the error bars, but reduces rapidly above $x = 0.10$, as shown in the inset of Figure 5b. Therefore, it indicates there exist two types of predominant electron-like charge carriers, one is active at low temperatures, the other at high temperatures [16]. As x increases, the high-temperature charge carriers get more and more dominant, while the low-temperature one becomes weaker, shifting the T^* to the lower temperatures. This behavior is possibly related with the p_x and p_y orbitals

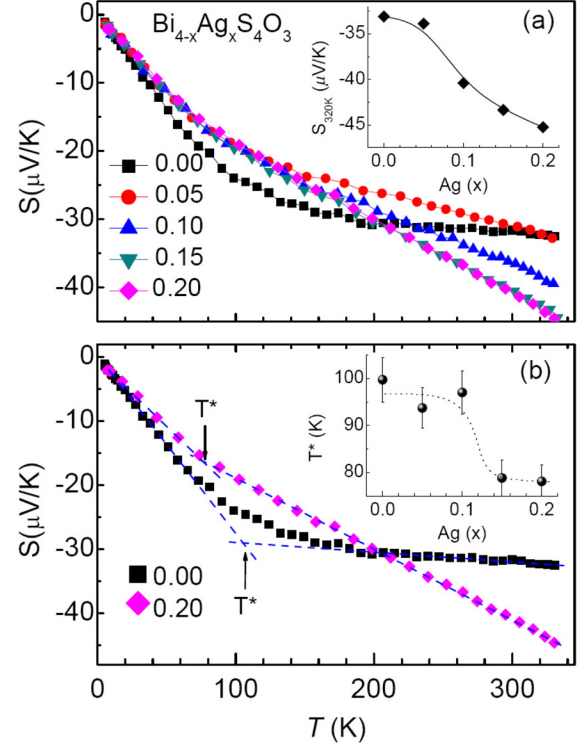


Fig. 5. (Color online) (a) Temperature dependence of the Seebeck coefficient for $\text{Bi}_{4-x}\text{Ag}_x\text{O}_4\text{S}_3$ ($0 \leq x \leq 0.2$). Inset shows the Seebeck coefficient at 320 K, $S_{320\text{K}}$. (b) The extrapolations (dotted lines) of both low-temperature and high-temperature linear $S(T)$ curves for $x = 0$ and 0.20 . The crossing temperature T^* for the two linear $S(T)$ parts is plotted in the inset as a function of x .

consisting the band structure near the E_F [7]. This result agrees in principle with the multiband feature of the Hall coefficient $R_H(T)$ data [8].

We are now focusing on the low-temperature linearly temperature dependent $S(T)$ since the superconductivity occurs at the low temperatures. Given a single band mode with an energy-independent relaxation time, the $S(T)$ can be written as $S(T) = \pi^2 \kappa_B^2 T / (3eE_F)$ [17], where κ_B is the Boltzman constant and E_F , the Fermi energy, corresponds to band maximum or minimum. The E_F can be estimated roughly using the slope of the low-temperature linear $S(T)$, dS/dT . So, a linear fitting was applied to all data below 50 K. The value of dS/dT is found to increase rapidly with increasing x when $x < 0.05$, and then saturates for $x \geq 0.10$ (see Fig. 6). It follows the evolution of the superconducting transition temperatures T_C^{onset} , defined as the onset of the dropping of the resistivity, and T_C^0 , where the magnetic susceptibility $-4\pi\chi(T)$ drops, as shown in the same figure. Assuming a rigid band, the decreasing dS/dT indicates a shift of the E_F to lower energy side. According to the theoretical calculation, for $x = 0$ the E_F is just at the position of a sharp peak in the density of state (DOS) originating mainly from the Bi-6p orbital within the BiS_2 layer [7]. Therefore, the shift of E_F will reduce the DOS at E_F , $N(E_F)$, leading to the reduction of T_C . The reduced $N(E_F)$ can also account for the

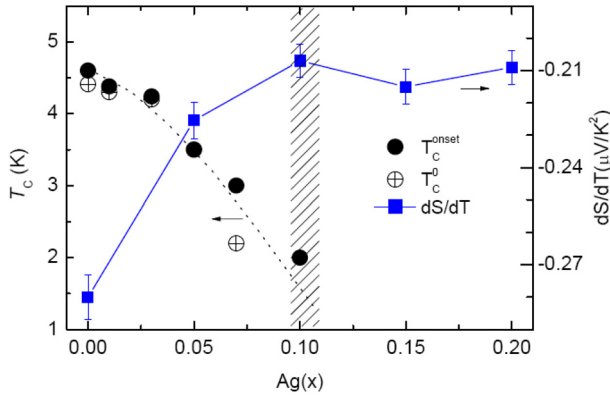


Fig. 6. (Color online) The slope dS/dT of the linearly temperature dependent $S(T)$ below 50 K, and the superconducting transition temperatures, T_C^{onset} and T_C^0 (see text for definitions) as a function of Ag composition. The hatched bar indicates the superconducting-nonsuperconducting boundary.

enhanced resistivity upon Ag doping. This result also indicates that the dopant Ag goes mainly to the BiS_2 layers, though Bi locates partially on the Bi_2O_2 layers. We note that the lattice effect on the electronic structure may be limited, because the observed lattice shrink is only $\sim 0.6\%$ along c -axis, and $\sim 0.2\%$ along $a(b)$ -axis, by the doping level of $x = 0.2$. The external pressure that compresses the lattice suppresses the T_C , but also reduces the normal state resistivity [13], contrary to the enhanced resistivity induced by Ag doping. Therefore, the suppression of superconductivity is mainly attributable to the modification of electronic structure, for instance, the shift of E_F mentioned above, though detailed mechanisms need further efforts, particularly from the theoreticians.

In summary, polycrystalline $\text{Bi}_{4-x}\text{Ag}_x\text{O}_4\text{S}_3$ ($0 \leq x \leq 0.2$) samples were prepared, and physical properties investigated. The superconductivity is suppressed by $x = 0.10$, above which the resistivity $\rho(T)$ shows the semiconductor-like temperature dependence, in contrast to the metallic behavior for lower doping levels. The analysis of Seebeck coefficient indicates a multiband behavior and the shift of E_F by Ag doping which may explain the suppression of T_C . All the results demonstrate unambiguously that the dopant Ag enters the $\text{Bi}_4\text{AgO}_4\text{S}_3$ lattice and the superconductivity is rather intrinsic.

This work was supported by the National Key Basic Research under contract No. 2011CBA00111 and the National Nature Science Foundation of China under contract Nos. 11274311, 11104279, 11174293, 51102240 and U1232139.

References

1. J.G. Bednorz, K.A. Muller, *Z. Physik B* **64**, 189 (1986)
2. Y. Kamihara, T. Watanabe, M. Hirano, H. Hosono, *J. Am. Chem. Soc.* **130**, 3296 (2008)
3. F.-C. Hsu, J.-Y. Luo, K.-W. Yeh, T.-K. Chen, T.-W. Huang, P.M. Wu, Y.-C. Lee, Y.-L. Huang, Y.-Y. Chu, D.-C. Yan, M.-K. Wu, *Proc. Natl. Acad. Sci. USA* **105**, 14262 (2008)
4. P.M. Aswathy, J.B. Anooja, P.M. Sarun, U. Syamaprasad, *Supercond. Sci. Technol.* **23**, 073001 (2010)
5. K. Ishida, Y. Nakai, H. Hosono, *J. Phys. Soc. Jpn* **78**, 062001 (2009)
6. G.R. Stewart, *Rev. Mod. Phys.* **83**, 1589 (2011)
7. Y. Mizuguchi, H. Fujihisa, Y. Gotoh, K. Suzuki, H. Usui, K. Kuroki, S. Demura, Y. Takano, H. Izawa, O. Miura, [arXiv:1207.3145](https://arxiv.org/abs/1207.3145) [*cond-mat.supr-con*] (2012)
8. S. Li, H. Yang, J. Tao, X.X. Ding, H.H. Wen, [arXiv:1207.4955](https://arxiv.org/abs/1207.4955) [*cond-mat.supr-con*] (2012)
9. S.G. Tan, L.J. Li, Y. Liu, P. Tong, B.C. Zhao, W.J. Lu, Y.P. Sun, *Physica C* **483**, 94 (2012)
10. H. Takatsu, Y. Mizuguchi, H. Izawa, O. Miura, H. Kadowaki, *J. Phys. Soc. Jpn* **81**, 125002 (2012)
11. S.K. Singh, A. Kumar, B. Gahtori, S. Kirton, G. Sharma, S. Patnaik, V.P.S. Awana, *J. Am. Chem. Soc.* **134**, 16504 (2012)
12. C.I. Sathish, K. Yamaura, [arXiv:1208.2818](https://arxiv.org/abs/1208.2818) [*cond-mat.supr-con*] (2012)
13. H. Kotegawa, Y. Tomita, H. Tou, H. Izawa, Y. Mizuguchi, O. Miura, S. Demura, K. Deguchi, Y. Takano, *J. Phys. Soc. Jpn* **81**, 103702 (2012)
14. J.A. Wilson, F.J. DiSalvo, S. Mahajan, *Adv. Phys.* **24**, 117 (1975)
15. K.F. Wang, H.C. Lei, C. Petrovic, *Phys. Rev. B* **84**, 054526 (2011)
16. W. Liu, J.W. Huang, Y.Z. Wang, X. Wang, Q.R. Feng, S.S. Yan, *Solid State Commun.* **118**, 575 (2001)
17. B. Gahtori, R. Lal, S.K. Agarwal, Y.K. Kuo, K.M. Sivakumar, J.K. Hsu, J.Y. Lin, A. Rao, S.K. Chen, J.L. MacManus-Driscoll, *Phys. Rev. B* **75**, 184513 (2007)